Influence of Dynamic Gap Junction Resistance on Impulse Propagation in Ventricular Myocardium: A Computer Simulation Study

Alexandra P. Henriquez,* Rolf Vogel,† Barbara J. Muller-Borer,‡ Craig S. Henriquez,§ Robert Weingart,† and Wayne E. Cascio‡

*Microelectronics Center of North Carolina, North Carolina Supercomputing Center, Research Triangle Park, North Carolina 27709 USA †Department of Physiology, University of Bern, CH-3012 Bern, Switzerland, ‡Department of Medicine, University of North Carolina at Chapel Hill, Chapel Hill 27599, and §Department of Biomedical Engineering, Duke University, Durham, North Carolina 27708 USA

ABSTRACT The gap junction connecting cardiac myocytes is voltage and time dependent. This simulation study investigated the effects of dynamic gap junctions on both the shape and conduction velocity of a propagating action potential. The dynamic gap junction model is based on that described by Vogel and Weingart (*J. Physiol. (Lond.). 1998, 510:177–189*) for the voltage- and time-dependent conductance changes measured in cell pairs. The model assumes that the conductive gap junction channels have four conformational states. The gap junction model was used to couple 300 cells in a linear strand with membrane dynamics of the cells defined by the Luo–Rudy I model. The results show that, when the cells are tightly coupled (6700 channels), little change occurs in the gap junction resistance during propagation. Thus, for tight coupling, there are negligible differences in the waveshape and propagation velocity when comparing the dynamic and static gap junction representations. For poor coupling (85 channels), the gap junction resistance increases 33 MΩ during propagation. This transient change in resistance resulted in increased transjunctional conduction delays, changes in action potential upstroke, and block of conduction at a lower junction resting resistance relative to a static gap junction model. The results suggest that the dynamics of the gap junction enhance cellular decoupling as a possible protective mechanism of isolating injured cells from their neighbors.

INTRODUCTION

In cardiac tissue, the electrical impulse propagates by means of local circuit currents. Local circuits represent closed loops involving four discrete structural elements: 1) membrane channels that carry the excitatory inward current, 2) the cytoplasm and gap junction in series representing the intracellular resistance pathway, 3) the membrane capacitance enabling the outward displacement current, and 4) the extracellular fluid acting as an extracellular resistance pathway. In essence, these four elements determine the speed of action potential propagation and the conditions leading to conduction failure (Cole et al., 1988; Joyner, 1981; Joyner et al., 1983, 1984; Fast and Kléber, 1995; Henriquez and Plonsey, 1987; Rudy and Quan, 1987; Quan and Rudy, 1990; Sahakian et al., 1992; Shaw and Rudy, 1995). Previous studies show that elements 1, 2, and 4 can be modified under pathological conditions, and thereby, affect the speed of and the safety factor for conduction.(Shaw and Rudy, 1997a,b,c; Spach and Heidlage, 1995) To better understand the complex interactions among these elements, a quantitative description of their properties is needed. With respect to 1, the data available on transmembrane currents allow a quantitative description of cardiac action potentials. With regard to 2, the behavior of current flow through cardiac gap junctions has been elucidated only recently. (Banach and Weingart, 1996; Bukauskas et al., 1995; Valiunas et al., 1997)

A number of models have been proposed to simulate conduction in discrete cardiac tissue (Joyner, 1982; Rudy and Quan, 1987; Quan and Rudy, 1990; Henriquez and Plonsey, 1987; Keener, 1991; Spach and Heidlage, 1992; Cai et al., 1994; Muller-Borer et al., 1994; Shaw and Rudy, 1995). These simulations and experimental studies (Spach et al., 1981; Rohr and Salzberg, 1994; Kucera et al., 1998; Rohr et al., 1997, 1998) provided a new picture of the complex interactions between current source and current sink factors. Although the computer simulation studies used different specific models to represent the membrane dynamics, all incorporated the gap junctions as passive elements with a constant resistance.

In this paper, we present a simulation study in which the fixed gap junction resistance (static model) is replaced by a variable resistance (dynamic model) to more accurately capture the dynamic electrical properties of the nexus. For this purpose, the dynamic gap junction model developed by Vogel and Weingart (1998) is integrated into a linear cable model consisting of ventricular cells with properties described by the Luo–Rudy I membrane model (Luo and Rudy, 1991). The dynamic gap junction model adopted is based on current measurements from isolated cell pairs (Banach and Weingart, 1996; Bukauskas et al., 1995; Valiunas et al., 1997). Measurements of multichannel currents show that the gap junction partially inactivates with time as a function of the transjunctional voltage whereas measurements of single-channel currents indicate that the gap junction channels are voltage gated and exhibit several conduc-

Received for publication 29 August 2000 and in final form 4 July 2001.

Address reprint requests to Alexandra Henriquez, Dept. of Biomedical Engineering, PO Box 90281, Duke University, Durham, NC 27708. Tel.: 919-660-5168; Fax: 919-684-4488; E-mail: sandyp@ncsc.org.

0006-3495/01/10/2112/10 $2.00

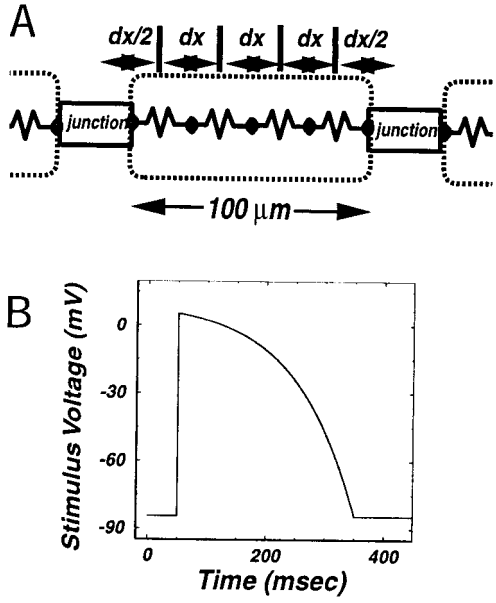

FIGURE 1 Elements of the mathematical model. (*A*) Schematic of the electrical analog used to model cardiac cells in a linear fiber. Each cell is 100 μm in length, with $dx = 25$ μm. The gap junction has either a variable resistance (dynamic model) or a constant resistor (static model). (*B*) A simulated action potential profile was used as voltage input to initiate propagation along the model. This voltage source was connected to the first node of the fiber with a 9.8-MΩ resistor.

tance states. Results from the simulations in this paper show that the dynamic gap junction has a significant effect on the shape of the action potential upstroke, the magnitude of the transjunctional delay, and the details of conduction failure when the number of connections is low, i.e., a large junction resistance. Preliminary results were presented previously in abstract form (Henriquez et al., 1998).

MATERIALS AND METHODS

Electrical analog

Propagation of an action potential was simulated in a 3-cm fiber of 300 cardiac cells. Each cardiac cell was 100 μm in length and 10 μm in radius and subdivided into discrete segments represented by five intracellular nodes (see Fig. 1 *A*). For uniform spacing between the nodes, three central compartments with a length $dx = 25$ μm, and two end compartments $dx/2 = 12.5$ μm were defined. The last node in each cell was connected to the first node of the adjacent cell with an element representing the gap junction. The intracellular resistivity of the cells was set to be 180 Ω/cm, yielding an effective resistance of 0.573 MΩ for each cell unit. The final node of the fiber was treated as a sealed end.

Numerical simulations established conservation of current at each node of the network using a system of nonlinear differential equations to describe the membrane dynamics and structure of the fiber. The system of differential equations was solved numerically at discrete time steps ($dt = 0.003$ ms) using a semi-implicit integration method, where the current flowing along the intracellular resistors was integrated using a trapezoidal integration method (Joyner et al., 1978) and the currents across the junctions and the cell membranes were incorporated with an explicit scheme.

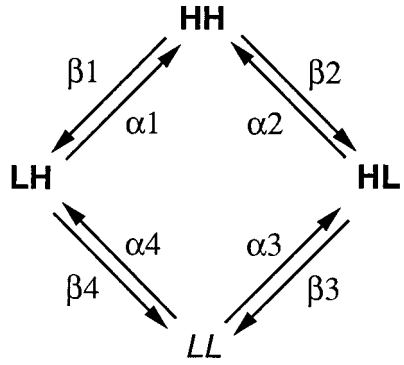

FIGURE 2 Diagram representing the properties of dynamic gap junction channels. Each gap junction consists of two hemichannels, which exist in either a high (H) or low (L) conductance state. This leads to the four conductance states HH, HL, LH, and LL. Transitions between states are represented by the respective rate constants α and β, which are nonlinear functions of the junction voltage (V_{junc}).

Overall, the integration scheme was first-order accurate in time and provided greater numerical stability than a pure explicit method.

Description of membrane current model

The ionic currents underlying the ventricular action potential were described using the Luo–Rudy I membrane model (Luo and Rudy, 1991). In brief, this mathematical model includes parameters that integrate the inward currents, i.e., I_{Na} and I_{si}, the outward currents, including the time-dependent I_K, time-independent I_{K1}, and the plateau phase current I_{Kp}, and a background current I_b. The initial conditions and the parameters used for the simulations are listed in the Appendix.

Description of gap junction models

The gap junctions were distributed uniformly along the length of the fiber. The gap junctions were represented by channels having resistive properties that were either constant (static model) or variable (dynamic model) with respect to voltage and time. With the static model, the channel conductance within the junction was fixed with respect to time and voltage. As such, the gap junction was represented as a linear, constant resistor. The dynamic model of the gap junction was implemented based on the mathematical model of Vogel and Weingart (1998) derived from experiments on cell pairs. (Bukauskas et al., 1995; Banach and Weingart, 1996; Valiunas et al., 1997) Current measurements revealed that the channels undergo voltage-dependent transitions from a main state to a residual state. From these observations, it follows that the conductance of the gap junction is dynamic and at any instant of time is a function of voltage across the gap junction. Each gap junction channel consists of two hemichannels in series. Each hemichannel can respond to the intercellular voltage, and thereby transition from a high (H) to a low (L) conductance state. Hence, each gap junction channel can reside in one of four functional states, i.e., HH, HL, LH, and LL. Four ordinary differential equations represented the transitions among the four states shown schematically in Fig. 2. The overall conductance of the gap junction (g_{gap}) is given by

$$g_{gap} = N_{chan} \cdot (n_{HH} \cdot g_{HH} + n_{HL} \cdot g_{HL} + n_{LH} \cdot g_{LH} + n_{LL} \cdot g_{LL}),$$

where N_{chan} represents the number of channels per gap junction, n_{HH}, n_{HL}, n_{LH}, and n_{LL} are the probabilities of the channels to be in the respective

states, and g_{HH}, g_{HL}, g_{LH}, and g_{LL} are the conductances of the channel states.

Connexin43 is the most abundant gap junction protein in ventricular muscle. Therefore, multichannel and single-channel data obtained for connexin43 were incorporated into the mathematical model (Banach and Weingart, 1996; Valiunas et al., 1997). In the dynamic gap junction model, both the rate coefficients (α and β) and the channel conductances (g_{HH}, g_{HL}, g_{LH}, and g_{LL}) are dependent on the transjunctional voltage, V_{junc} (see Fig. 2). The conductances for the homotypic states HH and LL were calculated analytically, whereas the conductances of the heterotypic states HL and LH were tabulated as a function of V_{junc}. The equations, constants, and parameters used for the simulations are listed in the Appendix.

The features of action potential propagation in fibers with the dynamic gap junction model were compared to those in fibers with the static model. The simulations were designed to compare propagation in the two types of fibers by varying the resistance of the junction over a broad range. In the static model, a single value of the gap junction resistance was assigned. The gap junction resistance for the static model, which did not vary with time or V_{junc} for a given case, was set to be equal to the baseline resistance for the corresponding dynamic model. Thus, for a given number of channels in the gap junction, the resistor value for the static model was set to be equal to the resistance of the dynamic model at rest (i.e., when the fiber is at rest conditions and the transjunctional voltage is zero). In the simulations with the dynamic gap junction model, the effective resistances of the junction were changed through the parameter N_{chan}.

Stimulus

Action potentials were triggered by a voltage stimulus applied through a 9.8-MΩ resistor connected in series to the first node of the first cell. The profile of the voltage stimulus (V_{stim}) mimicked the magnitude and duration of a standard action potential given by the expression

$$V_{stim}(t) = V_{peak} - (V_{peak} - V_{rest}) \cdot \exp[(t - t_{end})/\tau],$$

provided that $t_{start} < t < t_{end}$. $V_{stim} = V_{rest}$, otherwise where $V_{peak} = 10$ mV, $V_{rest} = -84.52$ mV, $\tau = 100$ ms, $t_{start} = 50$ ms, and $t_{end} = 300$ ms. The resulting stimulus is shown in Fig. 1 *B*.

RESULTS

Descriptive aspects of propagating action potentials

The first goal was to assess the role of decreasing the number of gap junction channels on the impulse propagation in a fiber of coupled cells. Of interest were the characteristics of propagation through the cell body and between cells across the gap junction. For this purpose, action potentials were evaluated at two nodes representing myoplasmic propagation, and two adjacent nodes representing transjunctional propagation. Propagation was evaluated in the middle of the fiber to avoid distortion of the signal secondary to end effects. Figure 3 shows propagating action potentials for conditions representing three different degrees of functional cell-to-cell coupling. The upper panel represents the control condition generating a normal conduction velocity of 50 cm/s. In the dynamic gap junction model, this required 6700 channels equivalent to a resting junction resistance of 2.0 MΩ. In the static model with a constant gap junction resistance of 2.0 MΩ the same propagation

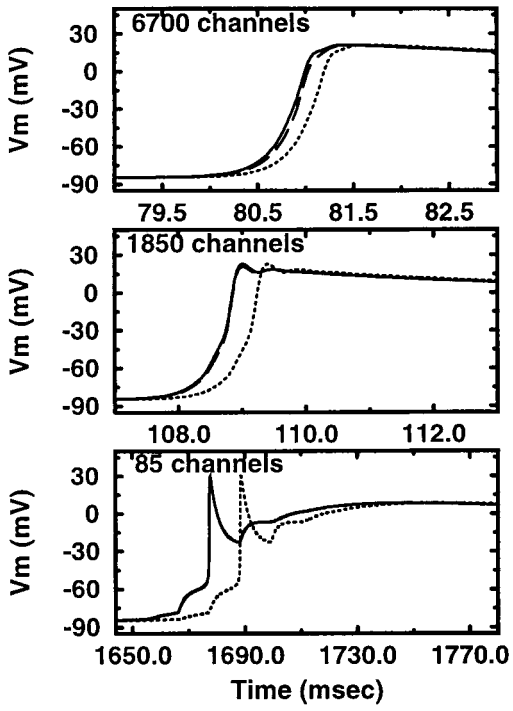

FIGURE 3 Role of gap junction resistance on the propagated action potential using the dynamic gap junction model. The three transmembrane voltage waveforms shown in each panel were calculated in the middle of the fiber, i.e., the first node of cell 150 (*solid line*), the last node of cell 150 (*dashed line*), and the first node of cell 151 (*dotted line*). Note the different time scales and the offsets in the three panels.

velocity was measured. The middle panel shows the action potentials corresponding to a 50% reduction in conduction velocity, i.e., 25.6 cm/s. In the dynamic gap junction model, this reduction in conduction velocity corresponds to a 3.6-fold reduction in the number of channels to 1850 channels, equivalent to a resting junction resistance of 7.37 MΩ. In the static model, a propagation velocity of 26.5 cm/s was observed with a junction resistance of 7.4 MΩ. The lower panel represents the conditions just before conduction block for the dynamic gap junction model. A minimum of 85 channels was required to sustain nondecremental propagation. Under these conditions, the propagation velocity was 0.91 cm/s and the resting junction resistance was 160.5 MΩ. By comparison, the critical limits for sustained conduction with the static model are reached at a larger gap junction resistance, i.e., 178 MΩ, but result in approximately the same minimum sustainable conduction velocity, i.e., 0.88 cm/s versus 0.91 cm/s.

The time courses shown in Fig. 3 emphasize the time delays within cells and across gap junctions during the upstroke of a propagating action potential. Each panel shows three curves obtained from: the first node of cell 150 (*solid curves*), the last node of cell 150 (*dashed curves*), and the first node of cell 151 (*dotted curves*). Therefore, the time interval between the first and second curves shows the delay

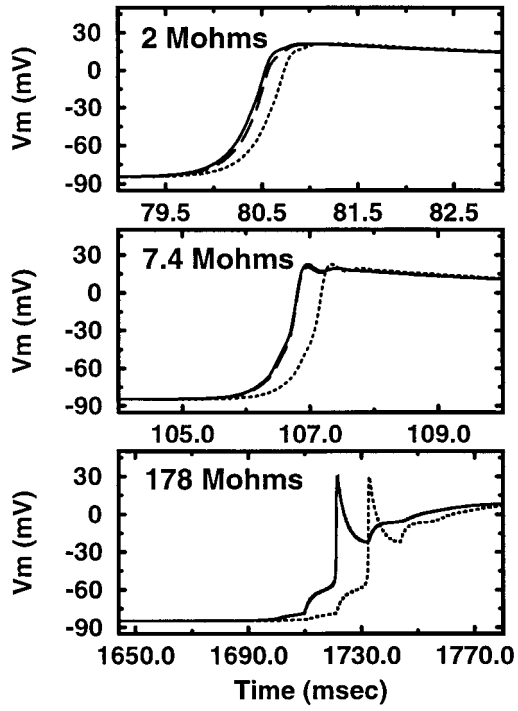

FIGURE 4 Propagation with static gap junctions model. Similar to Fig. 3, the three transmembrane voltage waveforms shown in each panel were calculated in the middle of the fiber, i.e., the first node of cell 150 (*solid line*), the last node of cell 150 (*dashed line*), and the first node of cell 151 (*dotted line*). The results plotted in the upper, middle, and lower panels are from fibers with static gap junctions of 2, 7.4, and 178 MΩ, respectively. Note the different time scales and the offsets in the three panels.

within a cell, whereas the time interval between the second and third curves shows the delay across the gap junction. A comparison of the three panels corresponding to 6700, 1850, and 85 dynamic gap junction channels leads to three key findings. First, the delay between the cells increases progressively as the number of channels decreases. Specifically, when determined at the incidence of dV/dt_{max}, it increased from 0.194 to 0.39 and 10.99 ms, respectively. Second, the delay across the myoplasm decreases as the number of channels is decreased. Delay decreased from 6.0 to 3.0 and 0 μs, respectively. Third, as the number of channels is decreased, the foot of the action potential is progressively slowed and a notch in the upstroke gradually develops. It is interesting to note that the triggered cell is electrotonically loaded in the forward direction and unloaded in the backward direction. The magnitude of this phenomenon increases as the number of channels is decreased. Close inspection of the signals in the lower panel indicates that activation of at least two previous cells contributes to the modification of the foot of the action potential, whereas activation of two or more subsequent cells contribute to the modifications of the early plateau phase.

The action potential upstrokes generated by the static gap junction model were also evaluated. Figure 4 shows the plot of the action potentials with expanded time scales for the fibers with 2.0, 7.4, and 178 MΩ. Propagation velocities in fibers with static resistances of 2.0, 7.4, and 178 MΩ were similar to those calculated in fibers with dynamic gap junction with 6700, 1850, and 85 channels, respectively. Analogous to the dynamic model, the transjunctional delays increased and the intracellular delays decreased as the junction resistance increased. The magnitude of the delays, however were different. The delay across the gap junction increased from 0.195 ms with 2.0 MΩ junctions, to 0.38 and 11.32 ms with 7.4 and 178 MΩ junctions, respectively, whereas the delay across the myoplasm decreased from 5 to 0 and 0 ms, respectively.

The dynamic and static models have slightly different effects on the time course of the propagating action potential, particularly for poor coupling. For the minimum number of channels in the dynamic gap junction model (85 channels), the baseline gap junction resistance is 160.5 MΩ and the propagation velocity is 0.91 cm/s. The static gap junction model with a junction resistance of 160.5 MΩ yields a propagation velocity of 1.4 cm/s. Propagation is sustained with static gap junction resistors as large as 178 MΩ, where the propagation velocity is 0.88 cm/s.

Figure 5 shows that the effect of the transient change in R_{junc} on the time course of the action potential is greatest during the early phases. Figure 5 *A* shows the early phase of action potentials calculated in the middle of a fiber with a dynamic gap junction consisting of 85 channels (*solid line*) and a static gap junction with a R_{junc} equal to the resting R_{junc} of the dynamic case, i.e., 160.5 MΩ (*dashed line*). The action potentials were aligned with respect to the incidence of dV/dt_{max}. This presentation emphasizes the electrical interactions with the adjacent cells. Because the take-off potential was comparable, the fast upstrokes of the action potentials were superimposable (dV/dt_{max} = 305.3 V/s and 342.7 V/s for the dynamic and static models, respectively). The dynamic model showed a slightly larger overshoot. This arises from a smaller current escape into the adjacent cells due to the transiently increased R_{junc}. With both gap junction models, the events before and after the fast upstroke of the action potential showed signs of forward and backward electrotonic interactions. These interactions were more prominent with the dynamic gap junction model. With regard to forward interactions, the depolarization during the foot of the action potential developed more slowly and lasted longer with the dynamic model. With regard to backward interactions, the notch of the action potential was more prominent and lasted longer with the dynamic model.

Figure 5 *B* shows the associated junction current, I_{junc}, for the two gap junction models. Negative and positive I_{junc} reflects current flow from and into the adjacent cells, respectively. I_{junc} exhibits a negative transient during the upstroke of the action potential, coincident in time but smaller in size with the dynamic model. This is consistent with the notion that less intercellular current flows during

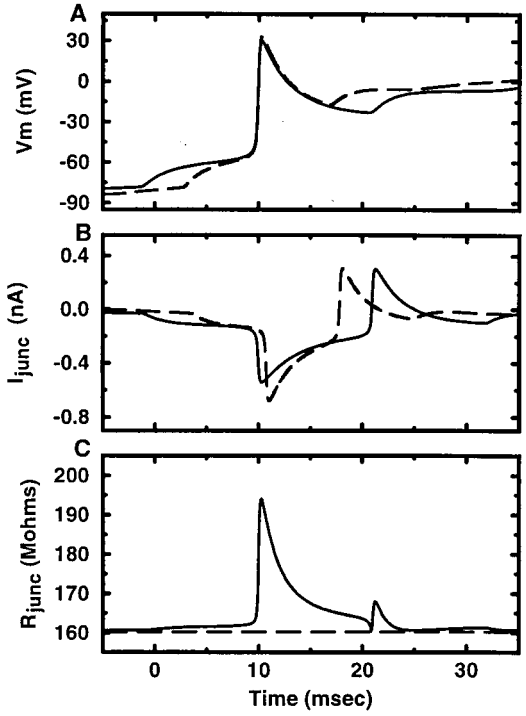

FIGURE 5 Factors that determine R_{junc} during the early phase of a propagated action potential. (*A*) Plots of membrane potential V_m versus time for propagating action potentials in a fiber with a dynamic (*solid line*) and static (*dashed line*) gap junction. (*B*) Plots of junction currents I_{junc} versus time. (*C*) Plots of R_{junc} versus time. All results were calculated at the same node in the middle of the fiber. The R_{junc} waveforms correspond to the largest effective gap junction resistance that sustained propagation with the dynamic model.

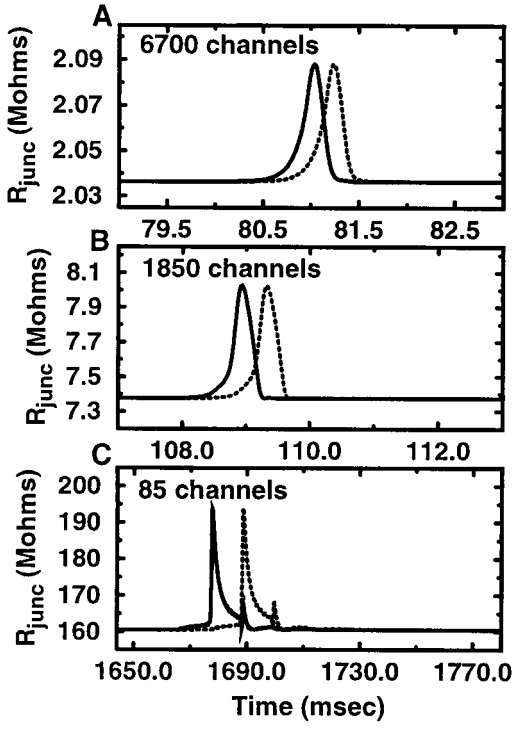

FIGURE 6 Changes in gap junction resistance during action potential propagation as a function of the number of gap junction channels. Plots are of R_{junc} versus time in a fiber with (*A*) 6700, (*B*) 1850, and (*C*) 85 dynamic channels. Each panel shows two waveforms calculated at different sites in the fiber: between cells 150 and 151 (*solid line*), and between cells 151 and 152 (*dotted line*). Time scales and offsets are the same as in Fig. 3.

this time interval. I_{junc} experienced positive transient during the notch of the action potential. It was delayed and marginally smaller with the dynamic model. This implies that R_{junc} is similar with both models. A comparison of the I_{junc} traces indicates that the two transients are similar in size and time course. Considering the size of the associated changes in V_m (see Fig. 5 *A*), this suggests that the increase in R_{junc} during the second I_{junc} transient is much smaller. During the foot of the action potential, a small negative I_{junc} developed. This current transient started later and lasted longer in the dynamic model.

Figure 5 *C* shows the time course of R_{junc} during the early phase of the action potential. Although R_{junc} remained constant with the static model, it showed a complex behavior with the dynamic model. R_{junc} increased dramatically in conjunction with the upstroke of the action potential. During the forward interactions, i.e., during the foot of the action potential, it showed a small gradual increase. During the backward interactions, i.e., during the notch of the action potential, it declined toward the reference level, first slowly and then abruptly. Associated with the secondary depolarization during the notch, R_{junc} showed a second transient increase, albeit of smaller size and shorter duration. Subsequently, there is a third transient with a significantly smaller transient.

Quantitative aspects of the junction resistance

In contrast to the static junction model, the dynamic gap junction model predicts a transient change in gap junction resistance, R_{junc}, during a propagated action potential, with a magnitude and time course that depends on the number of channels. Figure 6 shows the behavior of R_{junc} at two different sites of the fiber. The two curves shown correspond to adjacent gap junctions, the ones between cells 150–151 and cells 151–152. The three panels document the effects of the number of channels on the change in R_{junc}. The number of gap junction channels involved was the same as in Fig. 3. Decreasing the number of channels increases both R_{junc} at rest and during the action potential. The magnitude and duration of the change in R_{junc} during an action potential grows progressively as R_{junc} at rest is increased (note the different scales for R_{junc} in the three panels). Furthermore, there is a pronounced change in the contour of the transient increase in R_{junc}. As the number of channels is decreased, the falling phase becomes progressively slower when compared with the rising phase. In the case of very

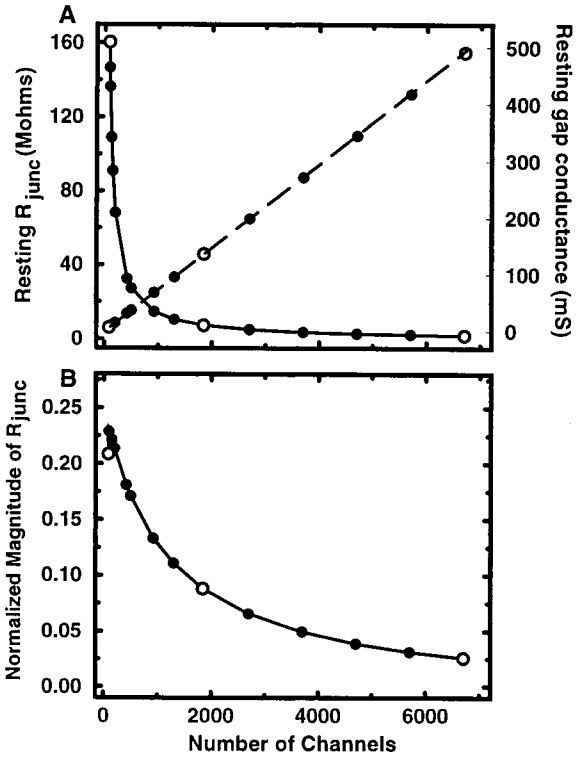

FIGURE 7 Junction resistance, R_{junc}, and conductance, $1/R_{junc}$, as a function of the number of gap junction channels. (*A*) The solid line, using the left axis, is a plot of the resting R_{junc} plotted as a function of number of channels, calculated for the dynamic gap junction. The dashed line, using the right axis, is a plot of the resting gap conductance, $1/R_{junc}$, as a function of the number of channels. (*B*) Plot of the normalized peak-to-peak change in R_{junc} as a function for the number of channels. Values were normalized with respect to the baseline R_{junc} for each case. Open circles in the plots refer to the cases shown in Figs. 3 and 5 (6700, 1850, and 85 channels). All values were calculated for the junction between cells 151 and 152 in the fiber.

limited cell-to-cell coupling as modeled by 85 channels, R_{junc} shows a secondary transient increase of smaller amplitude and shorter duration when compared with the initial transient, followed by an even smaller tertiary transient. The second and third transients reflect the sequential firing of the neighboring two cells along the strand.

The number of gap junction channels affects both R_{junc} at rest and during a propagated action potential. Figure 7*A* shows the plot of R_{junc} at rest versus the number of gap junction channels. The open circles refer to the analysis of the signals illustrated in Fig. 6. R_{junc} at rest is relatively constant when the number of channels in the junction exceeds 2000. As the number of channels decreases, the resting R_{junc} increases rapidly and becomes very steep below 750 channels. The two end points of the plot represent gap junctions with 6700 and 85 channels and correspond to a resting R_{junc} of 2.04 and 160.51 MΩ, respectively (see also Table 1). This translates into an 80-fold increase in R_{junc} at rest. Because of the dynamics of the channels, the resting R_{junc} of a gap junction cannot be inferred directly from the product of N_{chan} and g_{HH} (see Materials and Methods).

TABLE 1 Calculated quantities characterizing propagation in fibers with the dynamic gap junction model

Number of Channels	Resting Junction Resistance (MΩ)	Conduction Velocity (cm/s)	Delay across Junction (ms)
6700	2.04	50.0	0.19
5700	2.39	46.5	0.21
4700	2.90	42.5	0.23
3700	3.69	37.7	0.27
2700	5.05	31.7	0.31
1850	7.37	25.6	0.39
1300	10.50	20.6	0.48
925	14.75	16.3	0.61
500	27.29	10.2	0.99
420	32.48	8.7	1.14
200	68.22	4.2	2.36
150	90.96	3.0	3.35
100	136.43	1.6	6.31
85	160.51	0.91	10.99

Figure 7 *B* shows the plot of the peak change in R_{junc} associated with a propagating action potential versus the number of gap junction channels. The change in transient R_{junc} follows the same general pattern as the change in resting R_{junc} shown in Fig. 7 *A*. The two end points of the plot represent gap junctions with 6700 and 85 channels and correspond to peak changes in R_{junc} of 0.05 and 33.46 MΩ, respectively (see also Table 1). This change translates into a 670-fold increase in transient R_{junc}.

Table 1 summarizes the specific resistive parameters that influence the propagation of an action potential in the case of dynamic gap junction channels. The conduction velocity was calculated in the middle of the fiber over a length of 200 μm and two gap junctions, starting in the middle of a cell, and hence involving three cells. Measurements were related to the incidence of dV/dt_{max}. The time delay across a junction was determined from the incidence of dV/dt_{max} at the two nodes spanning the gap junction.

Quantitative aspects of conduction

An analysis of the conduction delays shows that the details of cell-to-cell action potential propagation for the dynamic junction differ from that seen with the static junction. Figure 8*A* compares plots of the conduction velocity of a propagating action potential versus resting R_{junc} for both the dynamic (*solid circles*) and the static (*open circles*) gap junction models. Qualitatively, the two curves show the same behavior. Quantitatively, the only significant difference appears at the points just before conduction block (*arrows*). In the fiber with dynamic gap junctions, the largest resting R_{junc} that sustained propagation along the

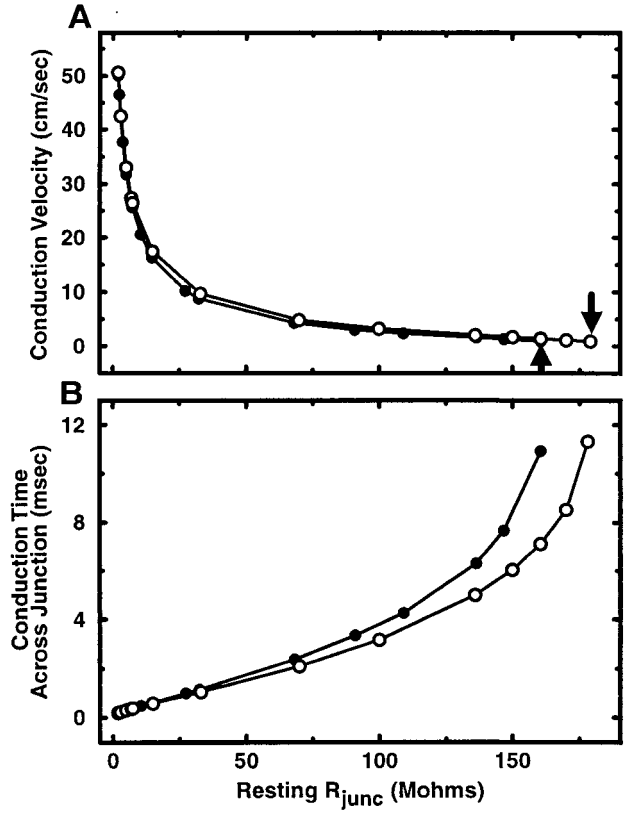

FIGURE 8 Comparison of conduction parameters between the static and dynamic model. (*A*) Plot of conduction velocity versus resting R_{junc} for fibers modeled with a dynamic (●) and static (○) gap junction. Arrows indicate the largest resistance that sustained action potential propagation to the end of the fiber. (*B*) Plot of conduction time across the junction versus resting R_{junc}. The two curves are shown for fibers with junctions of dynamic (●) and static (○) resistance.

entire fiber was 160.5 MΩ, corresponding to 85 channels and a conduction velocity of 0.91 cm/s. By contrast, the fiber with static gap junctions sustained propagation up to a junction resistance of 178.0 MΩ, corresponding to a conduction velocity of 0.88 cm/s. The difference between these two cases is due to the transient increase of 33.46 MΩ in R_{junc}, effectively increasing the overall junction resistance.

Figure 8 *B* shows plots of the conduction time across the gap junction versus resting R_{junc} both for the dynamic (*solid circles*) and the static (*open circles*) models. Greater insight into the mechanism of slowing and failure of propagation can be gained from analysis of the conduction time across the junction, i.e., the time an action potential takes to move from one cell to the next. The conduction time progressively increases as R_{junc} increases until propagation fails. The curves corresponding to the dynamic and static gap junctions begin to diverge as $R_{junc} > 50$ MΩ. The transjunctional conduction time increases at a faster rate in the fiber with dynamic junctions. The maximum conduction time for the dynamic gap junction was 10.99 ms with a resting R_{junc} of 160.5 MΩ. At the same R_{junc}, the delay was 7.11 ms for the static model. Hence, the transient increase in R_{junc} caused by a propagated action potential slows the conduction between two cells by 35%. Consequently, in the absence of this additional factor, conduction is sustained with a static R_{junc} of 178.0 MΩ and a transjunctional delay of 11.32 ms.

Table 1 also summarizes the data on R_{junc} at rest, R_{junc} during an action potential, the overall conduction velocity, and the conduction time across a gap junction. It serves to document the exact relationship of specific cases of channel numbers to resistive and conduction parameters.

DISCUSSION

The dynamic gap junction model used in this study is based on the physiological behavior of hemichannels derived from studies on pairs of neonatal rat hearts cells and of cells transfected with various connexins (Banach and Weingart, 1996; Bukauskas et al., 1995; Valiunas et al., 1997, 1999). The fundamental differences between this dynamic model and the static model used in previous propagation simulations (Joyner, 1982; Henriquez and Plonsey, 1987; Rudy and Quan, 1987; Keener, 1991; Shaw and Rudy, 1995; Spach and Heidlage, 1995) include: 1) The transjunctional voltage change during a propagating action potential introduces a transient increase in transjunctional resistance superimposed on the resting junction resistance; and 2) The resting junction resistance is higher than the resistance inferred from the number of channels and their unitary conductance, because, at rest, some channels reside in the low conductance state.

The main findings of this simulation study are that, under normal physiological conditions, characterized by strong cell-to-cell interaction and represented by a large number of gap junction channels in a one-dimensional fiber, the dynamic behavior of the gap junction contributes to a slight and physiologically insignificant increase in the junction resistance during the propagated action potential. This minor change does not affect the contour of the action potential, the speed of propagation along the fiber or the conduction delay across the gap junction. The insignificant difference in propagation is expected because there is no substantial transjunctional voltage when cells are electrically well coupled. As cell-to-cell electrical coupling is decreased, simulated by a decrease in the number of gap junction channels, the magnitude of the transjunctional voltage increases moderately, and the magnitude of the transient increase in junction resistance increases significantly. The transient increase in junction resistance associated with the propagation of the action potential results in greater delays in transjunctional conduction time and failure of conduction (conduction block) at lower resistances associated with the dynamic gap junction at rest when compared with the static gap junction model (Fig. 6). Under these conditions of conduction delay and block, the dynamic behavior of the

gap junction did not alter the qualitative nature of propagation, but rather affected the details of propagation failure (i.e., magnitude of resting R_{junc} and transjunctional delay) when compared with the static gap junction model.

Although these simulations demonstrate the significant dynamics that can occur in the gap junction for the cases near decremental propagation and conduction block, results with the dynamic gap junction model do not deviate from that observed with the more classical representation of gap junctions as constant resistors (Rudy and Quan, 1987). Note that, with 85 channels in the gap junction, the resistance can increase transiently by 30 MΩ simply from the upstroke of the normal action potential jumping from one cell to the next. However, the timing of this transient rise in the junction resistance is such that it does not significantly alter the dynamics of the propagation action potential.

The dynamic gap junction model may yield greater insight into the nature of electrical properties in cardiac tissue and impulse propagation under conditions associated with a marked decrease in the number or distribution of functional gap junction channels.(Spach, 1994; Peters and Wit, 2000) For example, pathological states such as myocardial hypertrophy (Cooklin et al., 1997), ischemia, and infarction (Severs, 1994) will reduce the number of functional channels. In addition, metabolic and ionic gradients distributed over small distances (e.g., the ischemic border zone) (Wilensky et al., 1986; Cascio et al., 1992) might support voltage gradients over small distances that will affect the transjunctional voltages, and thereby resistance, in a nonuniform way. It is possible that an increase in resistance could inhibit the propagation of ectopic electrical impulses, but this potential antiarrhythmic mechanism is yet unexplored. Using a realistic gap junction model that responds to such conditions in the environment may yield insight into mechanisms by which cardiac tissue responds and recovers to ischemic events and arrhythmias, particularly when inward calcium current mediate conduction and impedance mismatching are speculated to play an important role (Rohr and Kucera, 1997; Joyner et al., 1996).

One important limitation of the study is that propagation is simulated with the Luo–Rudy I model that lacks the correct kinetics of the activation and inactivation of excitatory Na and Ca currents. Because this model has been used successfully to describe general principles governing discontinuous impulse propagation under normal and abnormal conditions (Qu et al., 1999; Virag et al., 1998), it provides a means to investigate the basic principles of the dynamic gap junction kinetics on impulse propagation with only modest complexity. For weak coupling, the specifics of the calcium current and its impact on the time course of the plateau may change, for example, the minimum number of gap junctions needed for successful impulse transmission. (Shaw and Rudy, 1997c). Although we expect the general trends found in this study to be the same using any membrane model, the specific details of impulse conduction (and failure) will be affected by the time course of the ionic currents and also the dimensionality of the preparation. As a result, a study of the influence of dynamic gap junction kinetics on impulse propagation under pathological conditions or under the influence of membrane-active drugs that consider structural and membrane elements, will require its incorporation into a more physiologically accurate model (Luo and Rudy, 1994).

This work was supported by Microelectronics Center of North Carolina, North Carolina Supercomputing Center; P01 HL27430 from the National Institutes of Health, Heart, Lung and Blood Institute, Bethesda, Md.; DBI-99-74533 from the National Science Foundation; and the Swiss National Science Foundation (31–55297.98 to R.W.). R.V. was supported by a grant from the European Community (PL1427 to R.W.).

APPENDIX

Equations for the gap junction model with connexin43 hemichannels

Current

$$I_{junc}(t) = N_{chan}[n_{HH}g_{HH} + n_{LH}g_{LH} + n_{HL}g_{HL} + n_{LL}g_{LL}]V_{junc}(t) \quad \text{(A1)}$$

Kinetics for fractions of states

$$n_{HH} + n_{LH} + n_{HL} + n_{LL} = 1 \quad \text{(A2)}$$

$$\begin{aligned}
\frac{dn_{HH}}{dt} &= -(\beta_1 + \beta_2)n_{HH} + \alpha_1 n_{LH} + \alpha_2 n_{HL} \\
\frac{dn_{LH}}{dt} &= \beta_1 n_{HH} - (\alpha_1 + \beta_4)n_{LH} + \alpha_4 n_{LL} \\
\frac{dn_{HL}}{dt} &= \beta_2 n_{HH} - (\alpha_2 + \beta_3)n_{HL} + \alpha_3 n_{LL} \\
\frac{dn_{LL}}{dt} &= \beta_4 n_{LH} + \beta_3 n_{HL} - (\alpha_3 + \alpha_4)n_{LL}
\end{aligned} \quad \text{(A3)}$$

Rate coefficients

$$\alpha_1 = \frac{2\alpha_{coef}}{1 + \exp(-V_{LH1}/V_\alpha)} \quad \alpha_2 = \frac{2\alpha_{coef}}{1 + \exp(-V_{HL2}/V_\alpha)}$$

$$\alpha_3 = \frac{2\alpha_{coef}}{1 + \exp(-V_{LL1}/V_\alpha)} \quad \alpha_4 = \frac{2\alpha_{coef}}{1 + \exp(-V_{LL2}/V_\alpha)} \quad \text{(A4)}$$

$$\beta_1 = \beta_{coef}\exp(-V_{HH2}/V_\beta) \quad \beta_2 = \beta_{coef}\exp(-V_{HH2}/V_\beta)$$

$$\beta_3 = \beta_{coef}\exp(-V_{HL1}/V_\beta) \quad \beta_4 = \beta_{coef}\exp(-V_{LH2}/V_\beta), \quad \text{(A5)}$$

where the $V_{xy\#}$ refers to a hemichannel voltage. Specifically, this notation refers to the voltage across the first hemichannel (x) or the second hemichannel (y) of the composite channel xy.

Calculations for conductances and hemichannel voltages

$$g_{xy} = \frac{g_x g_y}{g_x + g_y} \quad g_x = \Gamma_x \exp(-V_{jx}/V_x), \qquad \text{(A6)}$$

where x and y refer to the state of the hemichannel (H or L) and V_{jx} refers to the voltage across hemichannel x. Eq. A6 for the total and hemichannel conductances can be solved iteratively with the equations for the hemichannel voltages,

$$V_{jx} = -V_j\left(\frac{g_y}{g_x + g_y}\right) \quad V_{jy} = V_j\left(\frac{g_x}{g_x + g_y}\right). \qquad \text{(A7)}$$

Constants and parameters

$$\Gamma_H = 146.6 \text{ pS} \quad \Gamma_L = 13.1 \text{ pS}$$

$$V_H = 145.9 \text{ mV} \quad V_L = 299 \text{ mV}$$

$$\alpha_{coef} = 181.5 \text{ s}^{-1} \quad \beta_{coef} = 0.007 \text{ s}^{-1}$$

$$V_\alpha = 8.437 \text{ mV} \quad V_\beta = 8.675 \text{ mV}$$

Initial conditions and parameters for LRI membrane model

$$[Na]_i = 18.0 \text{ mM} \quad [Na]_o = 140.0 \text{ mM}$$

$$[K]_i = 145.0 \text{ mM} \quad [K]_o = 5{,}4 \text{ mM}$$

$$[Ca]_i = 0.0002 \text{ mM} \quad [Ca]_o = 1.8 \text{ mM}$$

$$V_m = -84.52 \text{ mM} \quad \text{Temperature} = 37°\text{C}$$

REFERENCES

Banach, K., and R. Weingart. 1996. Connexin43 gap junctions exhibit asymmetrical gating properties. *Pflügers Arch*. 431:775–785.

Bukauskas, F. F., C. Elfgang, K. Willecke, and R. Weingart. 1995. Biophysical properties of gap junction channels formed by mouse connexin40 in induced cell pairs of transfected human HeLa cells. *Biophys. J.* 68:2289–2298.

Cascio, W. E., G.-X. Yan, and A. G. Kléber. 1992. Early changes in extracellular potassium in ischemic myocardium. The role of extracellular carbon dioxide accumulation and diffusion. *Circ. Res.* 70:409–422.

Cai, D., R. L. Winslow, and D. Noble. 1994. Effects of gap junction conductance on dynamics of sinoatrial node cells: two-cell and large-scale network models. *IEEE Trans. Biomed. Eng.* 41:217–231.

Cole, W. C., J. B. Picone, and N. Sperelakis. 1988. Gap junction uncoupling and discontinuous propagation in the heart. A comparison of experimental data with computer simulations. *Biophys. J.* 53:809–818.

Cooklin M., W. R. J. Wallis, D. J. Sheridan, and C.H. Fry. 1997. Changes in cell-to-cell electrical coupling associated with left ventricular hypertrophy. *Circ. Res.* 80:765–771.

Fast, V. G., and A. G. Kléber. 1995. Block of impulse propagation at an abrupt tissue expansion: evaluation of the critical strand diameter in 2- and 3-dimensional computer models. *Cardiovasc. Res.* 30:449–459.

Henriquez, A. P., B. J. Muller-Borer, C. S. Henriquez, R. Vogel, R. Weingart, and W. E. Cascio. 1998. A new physiologic gap junction model shows augmented cell-to-cell discontinuity during propagation in partially uncoupled fibers. *Circulation. 98* (Suppl. I):256.

Henriquez, C. S., and R. Plonsey. 1987. Effect of resistive discontinuities on waveshape and velocity in a single cardiac fiber. *Med. Biol. Eng. Comput*. 25:428–438.

Joyner, R.W. 1981 Mechanisms of unidirectional block in cardiac tissues. *Biophys. J.* 35:113–125

Joyner, R. W. 1982. Effects of the discrete pattern of electrical coupling on propagation through an electrical syncytium. *Circ. Res.* 50:192–200.

Joyner, R. W., R. Kumar, R. Wilders, H. J. Jongsma, E. E. Verheijck, D. A. Golod, A. C. G. van Ginneken, M. B. Wagner, and W. N. Goolsby. 1996. Modulating L-type calcium current affects discontinuous cardiac action potential conduction. *Biophys. J.* 71:237–245.

Joyner, R. W., J. Picone, R. Veenstra, and D. Rawling. 1983. Propagation through electrically coupled cells. Effects of regional changes in membrane properties. *Circ. Res.* 53:526–534.

Joyner, R. W., R. Veenstra, D. Rawling, and A. Chorro. 1984. Propagation through electrically coupled cells. Effects of a resistive barrier. *Biophys. J.* 45:1017–1025.

Joyner, R. W., M. Westerfield, J. W. Moore, and N. Stockbridge. 1978. A numerical method to model excitable cells. *Biophys. J.* 22:155–170.

Keener, J. P. 1991. The effects of discrete gap junction coupling on propagation in myocardium. *J. Theor. Biol.* 148:49–82.

Kucera, J. P., A. G. Kléber, and S. Rohr. 1998. Slow conduction in cardiac tissue. II. Effects of branching tissue geometry. *Circ. Res.* 83:795–805.

Luo, C.-H., and Y. Rudy. 1991. A model of the ventricular cardiac action potential. Depolarization, repolarization, and their interaction. *Circ. Res.* 68:1501–1526.

Luo, C.-H., and Y. Rudy. 1994. A dynamic model of the cardiac ventricular action potential. I. Simulations of ionic currents and concentration changes. *Circ. Res.* 74:1071–1096.

Muller-Borer, B. J., D. J. Erdman, and J. W. Buchanan. 1994. Electrical coupling and impulse propagation in anatomically modeled ventricular tissue. *IEEE Trans. Biomed. Eng.* 41:445–454.

Peters N. S., and A. L. Wit. 2000. Gap junction remodeling in infarction: does it play a role in arrhythmogenesis? *J. Cardiovasc. Electrophysiol.* 11:488–490.

Qu, Z., J. N. Weiss, and A. Garfinkel. 1999. Cardiac electrical restitution properties and stability of reentrant spiral waves: a simulation study. *Amer. J. Phys. Heart Circ. Phys.* 276:H269–H283.

Quan, R., and Y. Rudy. 1990. Unidirectional block and reentry of cardiac excitation: a model study. *Circ. Res.* 66:367–382.

Rohr, S., and J. P. Kucera. 1997. Involvement of the calcium inward current in cardiac impulse propagation: induction of unidirectional conduction block by nifedipine and reversal by BayK 8644. *Biophys. J.* 72:754–766.

Rohr, S., J. P. Kucera, V. G. Fast, and A. G. Kléber. 1997. Paradoxical improvement of impulse conduction in cardiac tissue by partial cellular uncoupling. *Science.* 275:841–844.

Rohr, S., J. P. Kucera, and A. G. Kléber. 1998. Slow conduction in cardiac tissue. I. Effects of a reduction of excitability versus a reduction of electrical coupling on microconduction. *Circ. Res.* 83:781–794.

Rohr, S., and B. M. Salzberg. 1994. Characterization of impulse propagation at the microscopic level across geometrically defined expansions of excitable tissue: multiple site optical recording of transmembrane voltage (MSORTV) in patterned growth heart cell cultures. *J. Gen. Physiol.* 104:287–309.

Rudy, Y., and W. L. Quan. 1987. A model study of the effects of the discrete cellular structure on electrical propagation in cardiac tissue. *Circ. Res.* 61:815–823.

Sahakian, A. V., G. A. Myers, and N. Maglaveras. 1992. Unidirectional block in cardiac fibers: effects of discontinuities in coupling resistance and spatial changes in resting membrane potential in a computer simulation study. *IEEE Trans. Biomed. Eng.* 39:510–522.

Severs, N. J. 1994. Pathophysiology of gap junctions in heart disease. *J. Cardiovasc. Electrophysiol.* 5:462–475

Shaw, R. M., and Y. Rudy. 1995. The vulnerable window for unidirectional block in cardiac tissue: characterization and dependence on membrane excitability and intercellular coupling. *J. Cardiovasc. Electrophysiol*. 6:115–131.

Shaw, R. M., and Y. Rudy. 1997a. Electrophysiologic effects of acute myocardial ischemia. A mechanistic investigation of action potential conduction and conduction failure. *Circ. Res.* 80:124–138.

Shaw, R. M., and Y. Rudy. 1997b. Electrophysiologic effects of acute myocardial ischemia: a theoretical study of altered cell excitability and action potential duration. *Cardiovasc. Res*. 35:256–272.

Shaw, R. M., and Y. Rudy. 1997c. Ionic mechanisms of propagation in cardiac tissue. Roles of the sodium and L-type calcium currents during reduced excitability and decreased gap junction coupling. *Circ. Res.* 81:727–741.

Spach, M. S. 1994. Changes in the topology of gap junctions as an adaptive structural response of the myocardium. *Circulation.* 90:1103–1106.

Spach, M. S., and J. F. Heidlage. 1992. A multidimensional model of cellular effects on the spread of electrotonic currents and on propagating action potentials. *Crit. Rev. Biomed. Eng*. 20:141–169.

Spach, M. S., and J. F. Heidlage. 1995. The stochastic nature of cardiac propagation at a microscopic level: electrical description of myocardial architecture and its application to conduction. *Circ. Res*. 76: 366–380.

Spach, M. S., W. T. Miller, D. B. Geselowitz, R. C. Barr, J. M. Kootsey, and E. A. Johnson. 1981. The discontinuous nature of propagation in normal canine cardiac muscle. Evidence for recurrent discontinuities of intracellular resistance that affect the membrane currents. *Circ. Res.* 48:39–54.

Valiunas, V., F. F. Bukauskas, and R. Weingart. 1997. Conductances and selective permeability of connexin43 gap junction channels examined in neonatal rat heart cells. *Circ. Res.* 80:708–719.

Valiunas, V., D. Manthey, R. Vogel, K. Willecke, and R. Weingart. 1999. Biophysical properties of mouse connexin30 gap junction channels studied in transfected human HeLa cells. *J. Physiol. (Lond.).* 519: 631–644.

Virag, N., J. M. Vesin, and L. Kappenberger. 1998. A computer model of cardiac electrical activity for the simulation of arrhythmias. *Pacing Clin. Electrophysiol.* 21:2366–2371.

Vogel, R., and R. Weingart. 1998. Mathematical model of vertebrate gap junctions derived from electrical measurements on homotypic and heterotypic channels. *J. Physiol. (Lond.).* 510:177–189.

Wilensky, R. L., J. Tranum-Jensen, R. Coronel, A. A. Wilde, J. W. Fiolet, and M. J. Janse. 1986. The subendocardial border zone during acute ischemia of the rabbit heart: an electrophysiologic, metabolic, and morphologic correlative study. *Circulation.* 74:1137–1146.